Journal of Solid State Chemistry 181 (2008) 1472–1479

Contents lists available at ScienceDirect

Journal of Solid State Chemistry

journal homepage: www.elsevier.com/locate/jssc

Thermal expansion of $Cr_{2x}Fe_{2-2x}Mo_3O_{12}$, $Al_{2x}Fe_{2-2x}Mo_3O_{12}$ and $Al_{2x}Cr_{2-2x}Mo_3O_{12}$ solid solutions

M. Ari [a], P.M. Jardim [a], B.A. Marinkovic [a,*], F. Rizzo [a], F.F. Ferreira [b]

[a] Departamento de Ciência dos Materiais e Metalurgia, Pontifícia Universidade Católica de Rio de Janeiro—PUC-Rio, Rua Marquês de São Vicente 225, Rio de Janeiro, RJ, Brazil
[b] Laboratório Nacional de Luz Síncrotron (LNLS), CP 6192, CEP 13083-970, Campinas, SP, Brazil

ARTICLE INFO

Article history:
Received 23 November 2007
Received in revised form
27 February 2008
Accepted 15 March 2008
Available online 27 March 2008

Keywords:
X-ray diffraction
Negative thermal expansion
Crystal structure
Molybdates

ABSTRACT

The transition temperature from monoclinic to orthorhombic and the thermal expansion of the orthorhombic phase were investigated for three systems of the family $A_2M_3O_{12}$: $Cr_{2x}Fe_{2-2x}Mo_3O_{12}$, $Al_{2x}Fe_{2-2x}Mo_3O_{12}$ and $Al_{2x}Cr_{2-2x}Mo_3O_{12}$. It was possible to obtain a single-phase solid solution in all studied samples ($x = 0$, 0.1, 0.3, 0.5, 0.7, 0.9 and 1).

A linear relationship between the transition temperature and the fraction of A^{3+} cations (x) was observed for each system. In all orthorhombic solid solutions studied here the observed thermal expansion was anisotropic. These anisotropic thermal expansion properties of crystallographic axes ***a***, ***b*** and ***c*** result in a low positive or near-zero overall linear coefficient of thermal expansion ($\alpha_l = \alpha_V/3$). The relationship between the size of A^{3+} cations in $A_2M_3O_{12}$ and the coefficient of thermal expansion is discussed. Near-zero thermal expansion of $Cr_2Mo_3O_{12}$ is explained by the behavior of Cr–O and Mo–O bond distances, Cr–Mo non-bond distances and Cr–O–Mo bond angles with increasing temperature, estimated by Rietveld analysis of synchrotron X-ray powder diffraction data.

1. Introduction

There are several studies about molybdates and tungstates of $A_2M_3O_{12}$ family reporting the phenomenon of negative thermal expansion (NTE) after phase transition from monoclinic to orthorhombic structure. Both structures consist of corner-sharing AO_6 octahedra and MO_4 tetrahedra. It appears that a transverse thermal motion of oxygen in the A–O–M linkage within lower-density orthorhombic structure produces NTE [1–4]. These structures present large chemical flexibility, which means that A^{3+} cation can be a transition metal or rare earth that accepts octahedral position, while M^{6+} is W^{6+} or Mo^{6+} [5,6]. This feature gives many options for cation substitution and recent literature reports several studies on the thermal expansion properties of tungstates and molybdates of $A_2M_3O_{12}$ family and their solid solutions [7–11]. Therefore, the extensive chemical flexibility makes this family rather promising for tailoring of new materials (solid solutions) with controllable coefficient of thermal expansion.

The $A_2M_3O_{12}$ family presents anisotropic thermal expansion and probably due to this reason there is currently a high discrepancy between the measurements of thermal expansion coefficients based on dilatometric and diffraction methods. Mary and Sleight [12] explained this difference by the formation of microcracks during specimen cooling and their elimination on heating, giving an extrinsic NTE contribution to the bulk thermal expansion. For example, the thermal expansion coefficient for $Al_2W_3O_{12}$ was reported as $+2.2\times10^{-6}/^{\circ}C$ based on X-ray diffraction (XRD) data [6], while $-3.0\times10^{-6}/^{\circ}C$ was measured by dilatometry [12]. Sivasubramanian et al. [13] corroborated this explanation by showing that after cooling, $In_2W_3O_{12}$ bulk specimen had enlarged its volume to about 0.1%, what was attributed to the formation of microcracks on cooling.

It seems from the literature that there is a correlation between cationic radii (A^{3+}) and thermal expansion coefficient of orthorhombic phases in $A_2M_3O_{12}$ family. This correlation is manifested in a way that the members of $A_2M_3O_{12}$ family with larger A^{3+} cations demonstrate more negative overall linear thermal expansion coefficient ($\alpha_l = \alpha_V/3$) than the ones with smaller A^{3+} [14]. In terms of axial thermal expansion, the phases with small A^{3+}, such as Al^{3+}, generally have two crystallographic axes with small negative or near-zero thermal expansion, while the third one shows large positive expansion [15]. On the other hand, the phases with large A^{3+}, such as $Y_2W_3O_{12}$ [15,16] and $Y_2Mo_3O_{12}$ [17,18], possess NTE along all three crystallographic axes. A classical rationalization of this correlation has been given by Forster et al. [14] in terms of small distortions of polyhedra (octahedra and tetrahedra) required for appearance of NTE in this structure. In the case of small (A^{3+}) cations, oxygen–oxygen repulsion is enhanced resulting in more rigid polyhedra and therefore these compounds usually do not show overall negative linear thermal expansion. On the other hand, the oxygen–oxygen

* Corresponding author. Fax: +51 21 35271248.
E-mail address: bojan@puc-rio.br (B.A. Marinkovic).

0022-4596/$ - see front matter © 2008 Elsevier Inc. All rights reserved.
doi:10.1016/j.jssc.2008.03.015

repulsion is diminished in octahedra with large A^{3+} cation resulting in a possibility of forming more distorted polyhedra on heating, allowing $A_2M_3O_{12}$ compounds with large A^{3+} cation to exhibit strong NTE in all crystallographic directions [14,15].

A relationship between phase transition temperature in $A_2M_3O_{12}$ family (from monoclinic $P2_1/a$ to orthorhombic $Pbcn$) and the cation (A^{3+}) electronegativity was proposed by Evans et al. [6]. It was suggested that as the electronegativity of the A^{3+} cation increases, the effective negative charge of oxygen anions decreases. Thus, in these cases the oxygen–oxygen repulsion decreases, while oxygen–oxygen attractive forces cause the transition to higher density monoclinic phase to occur at higher temperatures than in the phases with less electronegative A^{3+} cations.

In order to shed more light on the effect of the cation substitution on the thermal expansion coefficient and the temperature of phase transition from monoclinic to orthorhombic phase in the $A_2M_3O_{12}$ family, we studied through X-ray powder diffraction (XRPD) and thermal methods the following solid solutions: $Cr_{2x}Fe_{2-2x}Mo_3O_{12}$, $Al_{2x}Cr_{2-2x}Mo_3O_{12}$ and $Al_{2x}Fe_{2-2x}Mo_3O_{12}$ ($x = 0$, 0.1, 0.3, 0.5, 0.7, 0.9 and 1). As far as the authors are aware of, this is the first time that the thermal expansion properties of these solid solutions are reported. However, the pure orthorhombic $Al_2Mo_3O_{12}$, $Cr_2Mo_3O_{12}$ and $Fe_2Mo_3O_{12}$ were already studied through dilatometry and differential scanning calorimetry (DSC) by Tyagi et al. [19], being reported that all three phases have NTE. In the present work, thermal expansion coefficients are calculated for orthorhombic phases from high-resolution XRPD data, using a synchrotron radiation facility and it was demonstrated that these solid solutions, including the three pure phases, have near-zero or low positive overall linear thermal expansion, but not NTE as claimed by Tyagi et al. [19]. This difference has been addressed to the influence of the extrinsic contributions to thermal expansion recorded by dilatometry.

The general relationship between the size of cation A^{3+} and coefficient of thermal expansion of $A_2M_3O_{12}$ phases with orthorhombic structure has been also discussed. Near-zero thermal expansion of orthorhombic $Cr_2M_3O_{12}$ was discussed based on the behavior of Cr–O and Mo–O bond distances, Cr–Mo non-bond distances and Cr–O–Mo bond angles.

2. Experimental

$Cr_{2x}Fe_{2-2x}Mo_3O_{12}$, $Al_{2x}Cr_{2-2x}Mo_3O_{12}$ and $Al_{2x}Fe_{2-2x}Mo_3O_{12}$ solid solutions, ($x = 0$, 0.1, 0.3, 0.5, 0.7, 0.9 and 1) were produced by solid-state reaction from a stoichiometric mixture of Cr_2O_3 (Vetec, 99.5%), Al_2O_3 (ALCOA, 99.5%), Fe_2O_3 (Vetec, 99.5%) and MoO_3 (Fluka, 99.9%) powders, respectively. The reactants were preheated at 500 °C for 2 h, then weighed, activated mechanically by ball milling for 10 h and pressed at 250 MPa. The pellets were heated in alumina crucibles at 670 °C for 30 h and cooled down in the furnace.

XRPD patterns at room temperature were collected using a Siemens D-5000 diffractometer equipped with Cu sealed tube and graphite monochromator installed after the sample. The step-scanning mode was 0.02°/10 s. High-temperature XRPD (HTXRPD) of the samples were collected at four different temperatures always above the phase transition temperature from monoclinic to orthorhombic structure at the XRPD (D10B-XPD) beamline [20] of the Brazilian Synchrotron Light Laboratory (LNLS), placed after a dipolar source. X-rays of wavelength 1.3777(3) Å were selected by a double-bounce Si(111) monochromator, with water-refrigeration in the first crystal, while the second one is bent for sagittal focusing. The beam is vertically focused or collimated by a bent Rh-coated ultra low expansion glass mirror placed before the monochromator, which also provides filtering of high-energy photons (third- and higher-order harmonics). A vertically focused beam was used in the experiments in a spot of $\sim 1.0 \times 10^{-3}$ m (vertical) $\times \sim 2 \times 10^{-3}$ m (horizontal) into the sample position. The experiments were performed in the vertical scattering plane, i.e., perpendicular to the linear polarization of the incident photons. Wavelength and the zero point were determined from 11 well-defined reflections of the SRM640c silicon standard. The diffracted beam was analyzed with a Ge(111) crystal analyzer and detected with a Na(Tl)I scintillation counter with a pulse-height discriminator in the counting chain. The incoming beam was also monitored by a scintillation counter for normalization of the decay of the primary beam.

The powder sample was measured in flat-plate geometry and data were recorded at different temperatures for ~0.5 s at each 2θ in steps of 0.004° from 10° to 60°.

A calibration curve for the furnace (see Supplementary information) was obtained using a NIST Si sample and its cell parameter variation with temperature, provided by Yim and Paff [21]. This calibration curve was additionally verified and validated following the phase transition monoclinic to orthorhombic for different $A_2Mo_3O_{12}$ compounds and comparing it with DSC results (see Supplementary information).

A typical high-resolution XRPD pattern of the sample $Cr_2Mo_3O_{12}$ recorded at D10B-XPD beamline showing experimental, calculated and difference profile after Rietveld refinement, is illustrated in Fig. 1. The unit-cell and crystal structure parameters were refined from high-resolution diffraction patterns, through the Le Bail and Rietveld methods, using the program Topas-Academic and considering the space group $Pbcn$ for all orthorhombic phases. As the starting models for Rietveld refinements of investigated solid solutions, orthorhombic $Al_2Mo_3O_{12}$ and $Fe_2Mo_3O_{12}$ crystal structure descriptions from the ICSD files 80448 and 80449 were used. In the lack of a crystal structure description for the orthorhombic $Cr_2Mo_3O_{12}$, the crystal structure of $Fe_2Mo_3O_{12}$ (ICSD 80449) was used as the starting model for $Cr_2Mo_3O_{12}$. The refined crystal structures of orthorhombic $Cr_2Mo_3O_{12}$ at 420, 550, 650 and 740 °C have been deposited in the Inorganic Crystal Structure Database (ICSD) receiving numbers 418845, 418846, 418847 and 418848. Details of the Rietveld refinement are included in the Supplementary information.

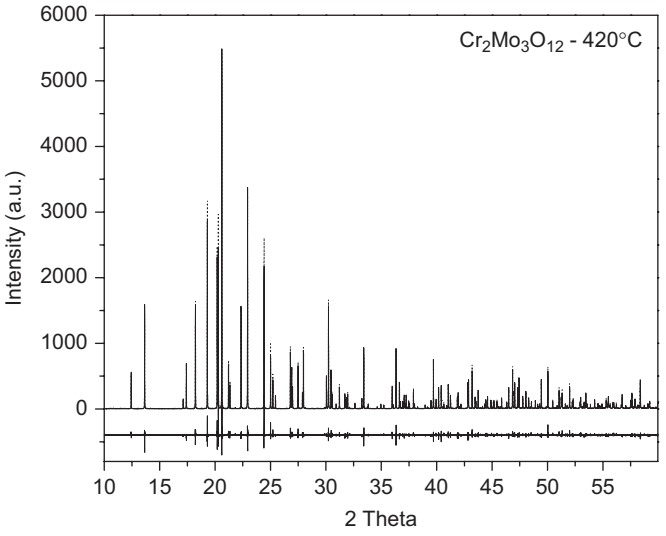

Fig. 1. High-resolution XRPD pattern for $Cr_2Mo_3O_{12}$ at 420 °C. Experimental profile (dot line), calculated and difference profiles (full lines).

Thermogravimetric (TG) analysis of $Al_2Mo_3O_{12}$, $Cr_2Mo_3O_{12}$ and $Fe_2Mo_3O_{12}$ were performed in air from room temperature up to 800 °C using a SETARAM thermal analyzer. The heating rate was 10 °C/min. The DSC analyses of all samples were performed in a Perkin-Elmer DSC-7 with a cycle including heating to 600 °C and cooling down to room temperature under argon atmosphere. The heating and cooling rates were 10 °C/min. The phase transition temperatures were determined using the PYRES software.

A scanning electron microscope (SEM) Zeiss DSM 960 equipped with an X-ray energy dispersive spectrometer was used in order to verify the phase composition of the synthesized samples.

3. Results and discussion

3.1. Monoclinic solid solutions

All obtained samples for $Cr_{2x}Fe_{2-2x}Mo_3O_{12}$, $Al_{2x}Cr_{2-2x}Mo_3O_{12}$ and $Al_{2x}Fe_{2-2x}Mo_3O_{12}$ solid solutions, appeared to be single-phased, as confirmed by room temperature XRPD and SEM. In accordance to that, it can be inferred that Fe^{3+} (0.645 Å), Cr^{3+} (0.615 Å) and Al^{3+} (0.535 Å) [22] can be totally substituted among themselves in $A_2Mo_3O_{12}$ structure due to the relatively small differences in their cationic radii.

The room temperature XRPD patterns of $Cr_{2x}Fe_{2-2x}Mo_3O_{12}$, $Al_{2x}Cr_{2-2x}Mo_3O_{12}$ and $Al_{2x}Fe_{2-2x}Mo_3O_{12}$ indicate that all solid solutions and pure phases appear in the monoclinic structure ($P2_1/a$). The variations of lattice parameters of $Cr_{2x}Fe_{2-2x}Mo_3O_{12}$, $Al_{2x}Cr_{2-2x}Mo_3O_{12}$ and $Al_{2x}Fe_{2-2x}Mo_3O_{12}$ solid solutions as a function of fraction (x) are shown in Fig. 2 and Supplementary information. It is observed that crystallographic axes ***a***, ***b***, ***c*** and volume V increase linearly with increasing of A^{3+} cation size and its content in the compound, while the β angle varies inversely. This dependence is in good agreement with the Vegard's law. A very similar trend was observed for $Al_{2-x}Sc_xW_3O_{12}$ solid solution in the orthorhombic structure [23].

3.2. Phase transition and hygroscopicity

The transition temperatures from monoclinic to orthorhombic structure for $Al_2Mo_3O_{12}$, $Cr_2Mo_3O_{12}$ and $Fe_2Mo_3O_{12}$ phases were reported [19] to be in the regions of 200–250, 350–400 and 500–550 °C, respectively, and this is in accordance with our findings (see Table 1 and Supplementary information). In the present work, however, the transition temperatures for the solid solutions: $Cr_{2x}Fe_{2-2x}Mo_3O_{12}$, $Al_{2x}Cr_{2-2x}Mo_3O_{12}$ and $Al_{2x}Fe_{2-2x}Mo_3O_{12}$ (Table 1 and Supplementary information) are reported as well. The DSC curves on heating show an endothermic peak for all specimens corresponding to the phase transition from monoclinic to orthorhombic. A linear relationship between the transition temperature and the fraction of A^{3+} cations (x) was observed for each system.

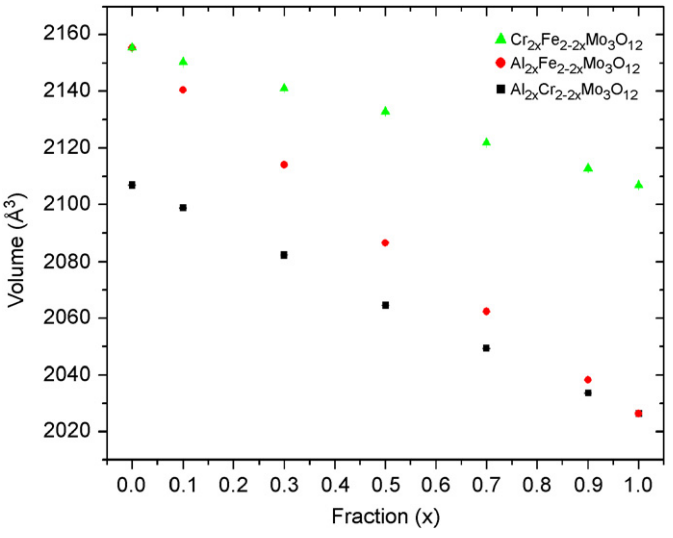

Fig. 2. Variation of volume of $Cr_{2x}Fe_{2-2x}Mo_3O_{12}$ (▲ symbols), $Al_{2x}Cr_{2-2x}Mo_3O_{12}$ (● symbols) and $Al_{2x}Fe_{2-2x}Mo_3O_{12}$ (■ symbols) in monoclinic structure at room temperature as a function of fraction (x). Standard uncertainties are included but are too small to appear in the graphs.

The relationship between the phase transition temperature and the electronegativity of A^{3+} cations, previously suggested by Evans et al. [6], was confirmed for each of the solid solutions studied here, considering electronegativity values for Fe^{3+}, Cr^{3+} and Al^{3+} (1.83, 1.66 and 1.61 [24], respectively) and the transition temperature of their solid solutions in $A_2Mo_3O_{12}$ family.

$Al_2Mo_3O_{12}$, $Cr_2Mo_3O_{12}$ and $Fe_2Mo_3O_{12}$ phases show a very low water loss from room temperature to 800 °C of 0.15, 0.09 and 0.25 wt%, respectively. Comparing these with rare-earth molybdates [17,18,25], that have weight losses at level of 6–8 wt% over the same temperature region, it could be inferred that Al, Cr and Fe-molybdates are not hydrated. This was an expected feature, based on the cation size differences between Al^{3+}, Cr^{3+} and Fe^{3+} on one side and rare earths on another, as well as on the fact that the monoclinic structure in $A_2M_3O_{12}$ family is denser than the orthorhombic one. Namely, the differences in A^{3+} cation sizes together with more dense monoclinic structure reflect over the size of intracrystalline channels of $A_2Mo_3O_{12}$ compounds. Therefore, smaller cations and denser structure form channels with smaller entrance, blocking at this manner water accommodation within the crystal structure.

3.3. Thermal expansion of orthorhombic solid solutions

The relationship between lattice parameters and temperature for $Cr_{2x}Fe_{2-2x}Mo_3O_{12}$, $Al_{2x}Cr_{2-2x}Mo_3O_{12}$ and $Al_{2x}Fe_{2-2x}Mo_3O_{12}$ solid solutions follows a linear dependence as can be seen in Fig. 3 and Supplementary information.

It is important to be observed (Fig. 4) that in all solid solutions studied here the coefficient of thermal expansion (α) along ***a*** direction is positive, varying between 6.25 and 7.96×10^{-6}/°C. On the other hand, the lattice parameter ***c*** shows low negative and near-zero thermal expansion, having a coefficient of thermal expansion α_c between −2.47 and 0.16×10^{-6}/°C. The thermal expansion properties of lattice parameter b are even more complex, being:

- low negative to near-zero for $Cr_{2x}Fe_{2-2x}Mo_3O_{12}$ solid solution, varying between -1.78×10^{-6} for $Cr_2Mo_3O_{12}$ and -0.62×10^{-6}/°C for $Fe_2Mo_3O_{12}$;

Table 1
Phase transition temperatures of $Cr_{2x}Fe_{2-2x}Mo_3O_{12}$, $Al_{2x}Cr_{2-2x}Mo_3O_{12}$ and $Al_{2x}Fe_{2-2x}Mo_3O_{12}$ solid solutions

$Cr_{2x}Fe_{2-2x}Mo_3O_{12}$		$Al_{2x}Cr_{2-2x}Mo_3O_{12}$		$Al_{2x}Fe_{2-2x}Mo_3O_{12}$	
x	T (°C)	x	T (°C)	x	T (°C)
0	512.5	0	403.02	0	512.5
0.1	500.3	0.1	374.04	0.1	484.1
0.3	483.5	0.3	327.79	0.3	430.2
0.5	465.2	0.5	283.71	0.5	368.6
0.7	441.2	0.7	244.31	0.7	305.3
0.9	418.2	0.9	214.4	0.9	239.8
1	403	1	200.22	1	200.2

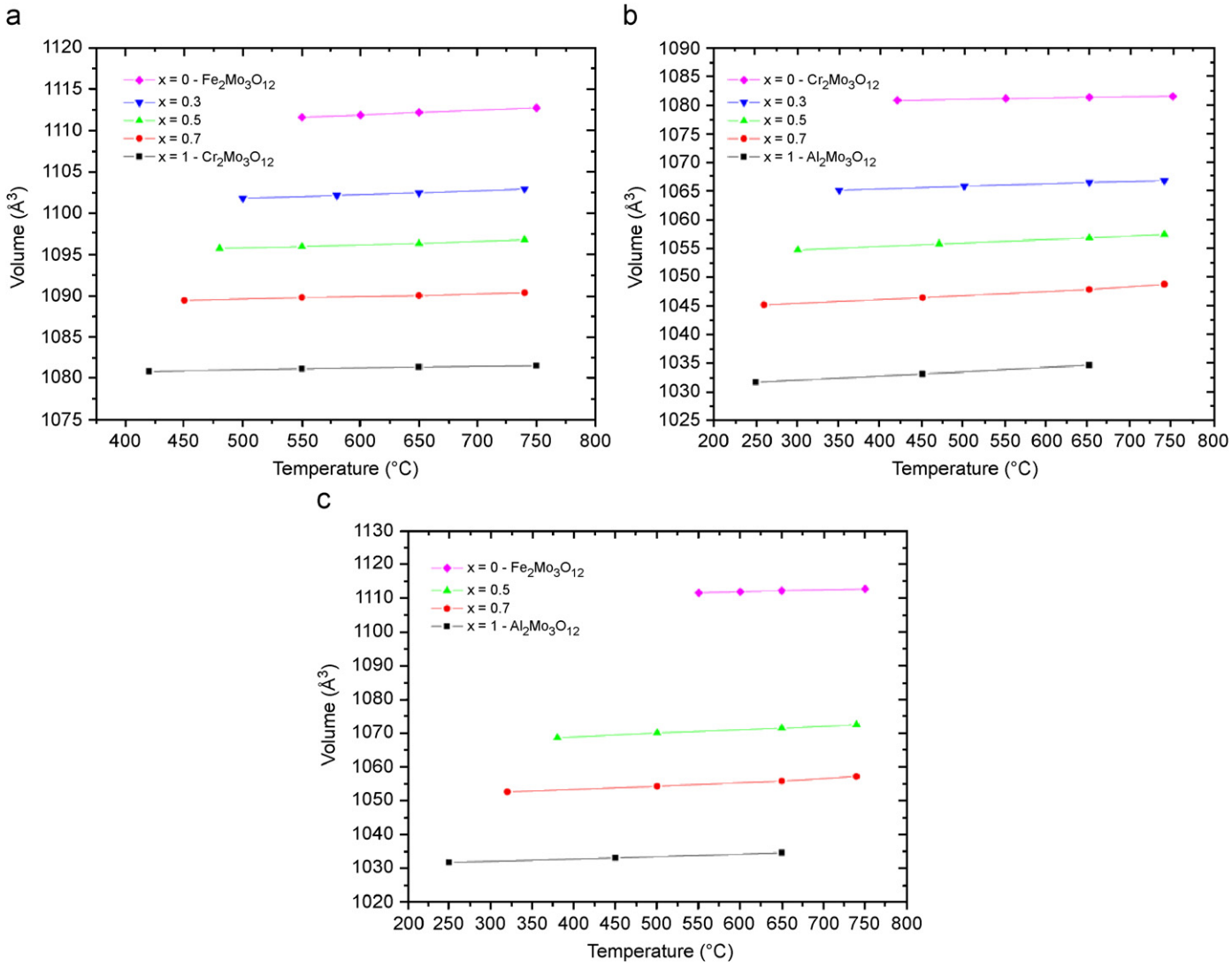

Fig. 3. Variation of volume of (a) $Cr_2Fe_{2-2x}Mo_3O_{12}$, (b) $Al_2Cr_{2-2x}Mo_3O_{12}$, and (c) $Al_2Fe_{2-2x}Mo_3O_{12}$ solid solutions vs. temperature. Standard uncertainties are included but are too small to appear in the graphs.

- near-zero for $Al_{2x}Cr_{2-2x}Mo_3O_{12}$ solid solution, varying between -0.63×10^{-6} for $Cr_{1.4}Al_{0.6}Mo_3O_{12}$ and $0.71\times10^{-6}/°C$ for $Al_{1.4}Cr_{0.6}Mo_3O_{12}$ and
- low positive for $Al_{2x}Fe_{2-2x}Mo_3O_{12}$ being $2.01\times10^{-6}/°C$ for $AlFeMo_3O_{12}$.

These thermal expansion properties of crystallographic axes ***a***, ***b*** and ***c*** result in a low positive or near-zero overall linear coefficient of thermal expansion ($\alpha_l=\alpha_V/3$) for the studied $Cr_{2x}Fe_{2-2x}Mo_3O_{12}$, $Al_{2x}Cr_{2-2x}Mo_3O_{12}$ and $Al_{2x}Fe_{2-2x}Mo_3O_{12}$ solid solutions (Fig. 4). Standard deviations for calculated α values are very small as can be seen from Fig. 4, which enables reliable comparison among different solid solutions studied.

Overall linear coefficient of thermal expansion (α_l) for $Fe_2Mo_3O_{12}$ has been already reported by Cheng et al. [9] as $1.14\times10^{-6}/°C$, while Yang et al. [26] reported for $Cr_2Mo_3O_{12}$ an $\alpha_l=1.61\times10^{-6}/°C$, both α_l being calculated from conventional XRD data. However, overall linear coefficient of thermal expansion (α_l) for $Fe_2Mo_3O_{12}$ and $Cr_2Mo_3O_{12}$ calculated from our high-resolution XRPD patterns in the present work were $\alpha_l=1.72\times10^{-6}$ and $0.67\times10^{-6}/°C$, respectively. The observed discrepancies can be attributed to the following contributions. The first one can be errors in the temperature calibration of the furnace. Secondly, it can be the difference in the resolution of synchrotron and conventional XRD patterns. This can be proved by simulation of high- and low-resolution XRD patterns of a same $A_2Mo_3O_{12}$ crystal structure, where the standard uncertainties of the cell parameters calculated by Rietveld refinement are higher for the low-resolution pattern and also different cell parameter values were obtained for each case. The third contributions can be the manner how coefficient of thermal expansion is calculated, since there are different ways to perform this calculation. Here, we used natural logarithmic plots ($\ln V$ versus T, for example) and linear regression (with R values superior to 99%) to calculate coefficient of thermal expansion form the inclination. Only in some cases of α calculated for ***b***-axis R-values were lower than 99%. On the other hand, Tyagi et al. [19] measured the $Al_2Mo_3O_{12}$ compound by dilatometry and obtained a low negative linear thermal expansion ($\alpha_l=-2.83\times10^{-6}/°C$), and a very strong negative linear thermal expansion for $Cr_2Mo_3O_{12}$ and $Fe_2Mo_3O_{12}$ ($\alpha_l=-9.39\times10^{-6}$ and $-14.82\times10^{-6}/°C$, respectively). Actually, it can be generalized for the $A_2M_3O_{12}$ family (Fig. 5) that there are large misfits between the linear coefficients of thermal expansion (CTE) measured by diffraction and dilatometric methods. There are probably several extrinsic sources causing discrepancy, but by

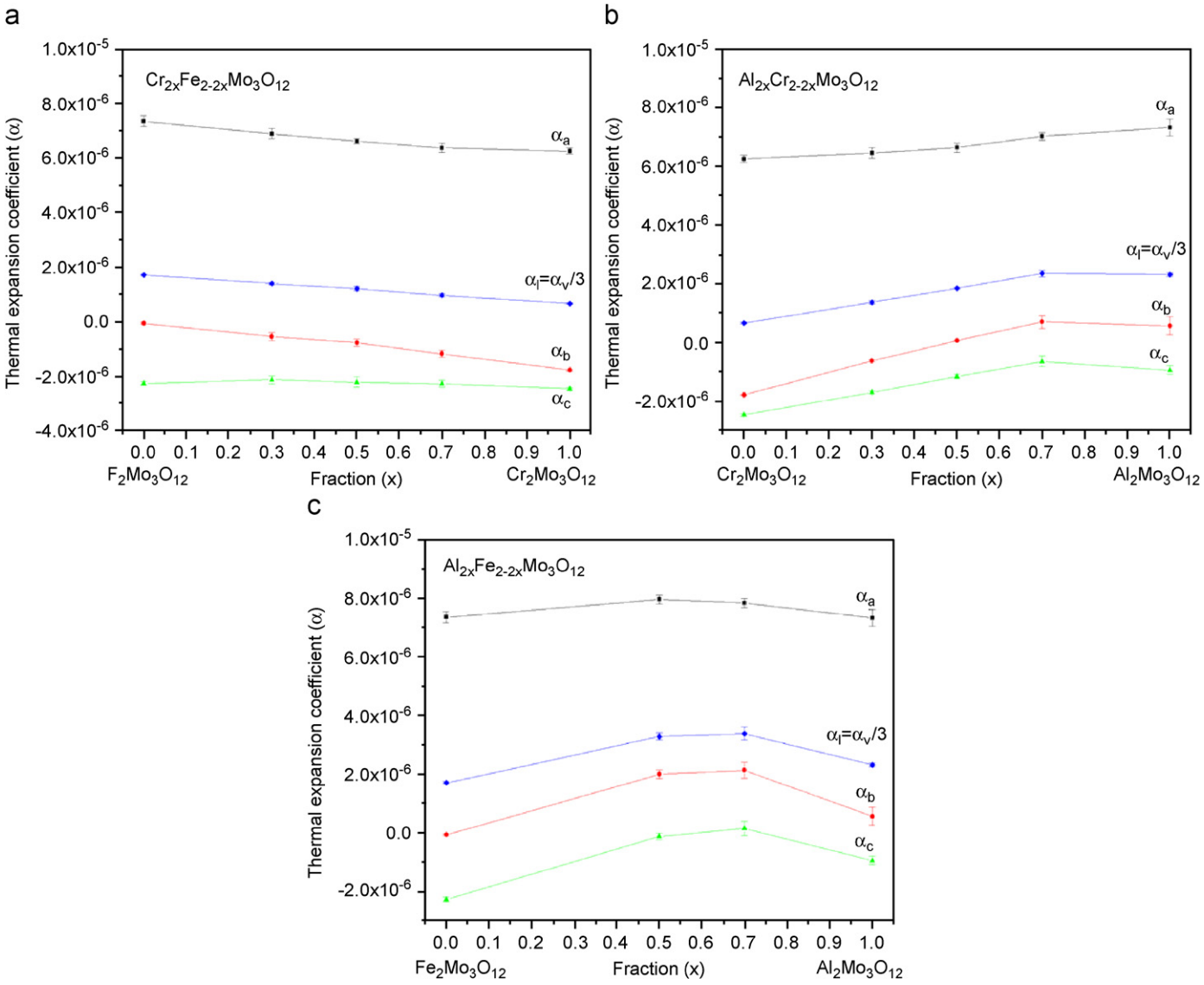

Fig. 4. Thermal expansion coefficients for (a) $Cr_2Fe_{2-2x}Mo_3O_{12}$ solid solution as a function of Cr^{3+} content, (b) $Al_2Cr_{2-2x}Mo_3O_{12}$ solid solution as a function of Al^{3+} content and (c) $Al_2Fe_{2-2x}Mo_3O_{12}$ solid solution as a function of Al^{3+} content.

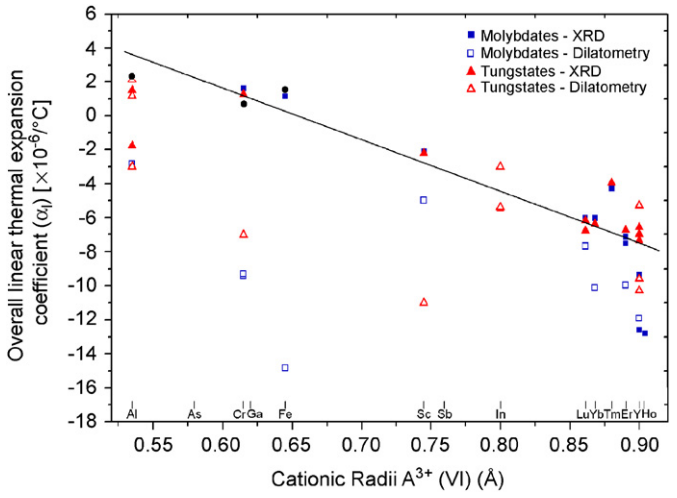

Fig. 5. Overall linear thermal expansion coefficients for molybdates and tungstates of $A_2M_3O_{12}$ family, obtained by X-ray or neutron diffraction and dilatometry [6–19,28,31,32,34–36]; results reported in this work (●). The full line is a guide for the eyes.

far the most cited one is the formation of microcracks on cooling due to the anisotropic thermal expansion of these phases. This seems to be a rather reasonable explanation, considering that in the cubic ZrW_2O_8 family, dilatometric and diffraction measurements of linear CTE are in good agreement [27]. Certainly, in some cases, another source of discrepancy can be the use of not sufficiently well sintered pellets for dilatometric measurements. However, a more systematic study is necessary to fully understand this phenomenon, especially having in mind a potential application of materials of the $A_2M_3O_{12}$ family with tailored intrinsic coefficient of thermal expansion, where extrinsic contribution to thermal expansion must be minimized.

In Fig. 5, all published overall linear CTE for orthorhombic $A_2M_3O_{12}$ family obtained through diffraction methods (closed squares ■ for molybdates and closed triangles ▲ for tungstates) as a function of A^{3+} cation radii size, together with dilatometric results, are plotted. The majority of the overall linear CTE, plotted in Fig. 5, has been calculated for the temperature interval between room temperature and 800 °C (see Supplementary information for details). This plot confirms the general trend for overall linear CTE for orthorhombic $A_2M_3O_{12}$ family as dependent on A^{3+} cation radii size. However, tailoring intrinsic thermal expansion properties for

$A_2M_3O_{12}$ phases and their solid solutions through substitutions of cation A^{3+}, using the rationalization that larger A^{3+} cations provoke more NTE and vice-versa, is not always straightforward (Fig. 5). Namely, our results indicate that $Cr_2Mo_3O_{12}$ and $Fe_2Mo_3O_{12}$ do not exactly follow the established relationship between overall linear CTE and the size of A^{3+} cation. This means that $Cr_2Mo_3O_{12}$ has lower overall linear CTE ($\alpha_l = 0.67 \times 10^{-6}/^{\circ}C$) than $Fe_2Mo_3O_{12}$ ($\alpha_l = 1.72 \times 10^{-6}/^{\circ}C$), although the size of Cr^{3+} in octahedral coordination is smaller (0.615 Å) than the size of Fe^{3+} (0.645 Å) [22] in the same coordination. Similar discrepancy from the general relationship was recently noticed for $Tm_2Mo_3O_{12}$ and $Tm_2W_3O_{12}$ phases that show much lower NTE ($\alpha_l = -4.03 \times 10^{-6}$ and $-3.95 \times 10^{-6}/^{\circ}C$) [28] than other rare-earth molybdates and tungstates of the $A_2M_3O_{12}$ family (see Fig. 5). As a matter of fact, some of our results on cationic substitution in the $Cr_{2x}Fe_{2-2x}Mo_3O_{12}$, $Al_{2x}Cr_{2-2x}Mo_3O_{12}$ and $Al_{2x}Fe_{2-2x}Mo_3O_{12}$ solid solutions reveal that overall linear CTE does not always change (Fig. 4) according to A^{3+} size effect. As can be seen from Fig. 4a overall linear coefficient of thermal expansion in $Cr_{2x}Fe_{2-2x}Mo_3O_{12}$ changes in a linear way with the increase of the fraction (x), of larger A^{3+} cation, although in the opposite manner considering the cation sizes of Cr^{3+} and Fe^{3+}, as previously discussed. For the $Al_{2x}Cr_{2-2x}Mo_3O_{12}$ system, a decrease of α_l with the increase of fraction (x) of the larger A^{3+} is observed (Fig. 4b). However, the $Al_{2x}Fe_{2-2x}Mo_3O_{12}$ system shows a more complex dependence between overall linear coefficient of thermal expansion and the fraction (x) (Fig. 4c). In this system, $AlFeMo_3O_{12}$ and $Al_{1.4}Fe_{0.6}Mo_3O_{12}$ phases have more positive α_l than the pure phases ($Al_2Mo_3O_{12}$ and $Fe_2Mo_3O_{12}$). Actually, in recent literature on thermal expansion in $A_2M_3O_{12}$ family there are also few examples of such unexpected behavior of overall linear coefficient of thermal expansion as a function of fraction (x) of larger A^{3+} cations [7,29]. Peng et al. [7] reported for the $Y_{2-x}Nd_xW_3O_{12}$ system that when the fraction (x) of larger cation Nd^{3+} is increased from $x = 0.1$ to 0.4, α_l became less negative, instead of becoming more negative. Similar was observed for $Y_{2-x}Sm_xW_3O_{12}$ system [29]. However, for some other systems such as: $Nd_{2-x}Er_xW_3O_{12}$ [8], $Fe_{2-x}Er_xMo_3O_{12}$ [9], $Er_{2-x}Ce_xW_3O_{12}$ [10] and $Er_{2-x}Sm_xW_3O_{12}$ [11], the overall linear coefficient of thermal expansion become more negative with increasing values of the fraction (x) of larger cation, as can be expected from the general trend observed in Fig. 5. Considering our results on thermal expansion of $Cr_2Mo_3O_{12}$ and the reports from literature on $Y_{2-x}Nd_xW_3O_{12}$, $Y_{2-x}Sm_xW_3O_{12}$, $Tm_2Mo_3O_{12}$ and $Tm_2W_3O_{12}$ [7,28,29], it occurs that in some systems exists another factor, apart from A^{3+} cationic size, that can influence their thermal expansion properties. This another factor for $A_2M_3O_{12}$ system can be suggested based on Chapman et al. [30] study on the effect of M^{2+} substitution on the magnitude of the NTE for a family of Prussian Blue analogs, $M^{2+}Pt^{4+}(CN)_6$ for M^{2+} = Mn, Fe, Co, Ni, Cu, Zn, Cd. The authors found that NTE varies widely with M^{2+} substitution and explained this variation in thermal expansion being primarily due to the different bond strengths of M^{2+}-cyanide binding interaction, i.e., decreased structural flexibility is associated with stronger M^{2+}–N bonds resulting in reduced NTE. It can be therefore suggested that the strength of A^{3+}–O bonds in $A_2M_3O_{12}$ also plays a role in the NTE behavior of these materials. This might explain unexpected observation that $Cr_2Mo_3O_{12}$ shows a lower overall linear CTE than $Fe_2Mo_3O_{12}$.

The changes of crystal structure details of $Cr_2Mo_3O_{12}$ orthorhombic phase as a function of temperature (from 420 to 740 °C), such as bonding distances Cr–O, Mo–O, non-bonding distance Cr–Mo and angles Cr–O–Mo, were evaluated by the Rietveld method. Due to the large crystallite sizes of $Al_2Mo_3O_{12}$ and $Fe_2Mo_3O_{12}$ it was not possible to perform Rietveld refinements on the diffraction patterns of these two phases. Table 2 resumes

Table 2
Rietveld reliability factors for the refined diffraction patterns of $Cr_2Mo_3O_{12}$

Temperature (°C)	R_B (%)	Gof	R_{wp} (%)	R_{exp} (%)
420	3.17	1.28	21.25	16.52
550	3.81	1.30	21.37	16.43
650	3.69	1.30	21.26	16.36
740	4.15	1.31	21.38	16.32

Number of data points was 12,500, number of refined parameters was 42 and number of considered diffraction lines was 225 for all four temperatures.

Rietveld reliability factors for the refined diffraction patterns, while all details of Rietveld refinement are given in Supplementary information. In some previous detailed neutron diffraction studies of $A_2M_3O_{12}$ phases ($Sc_2W_3O_{12}$ [31], $Sc_2Mo_3O_{12}$ [32] and $Y_2W_3O_{12}$ [16]) it was generally established that W–O and Mo–O apparent bond lengths undergo contraction during heating. The same occurred for Mo–O in $Cr_2Mo_3O_{12}$ phase [d_{av}(Mo–O) = $1.7249 - 4.25 \times 10^{-5}$ T Å, calculated by linear regression], as illustrated in Fig. 6a. This is actually an expected feature considering that Mo^{6+}–O bonds are extremely strong, having practically a zero thermal expansion especially when Mo^{6+} occupies tetrahedral sites [33], and the possibility of existence of transverse vibration modes of oxygen atoms, as it is the case in $A_2M_3O_{12}$ family. In the case of $Sc_2W_3O_{12}$, $Sc_2Mo_3O_{12}$ and $Y_2W_3O_{12}$ the authors [16,31,32] also found that Y–O and Sc–O (in $Sc_2W_3O_{12}$) bond lengths do not change significantly with increasing temperatures, while in the case of $Sc_2Mo_3O_{12}$, the Sc–O bond length even underwent an observable apparent contraction [d_{av}(Sc–O) = $2.0973 - 2.7 \times 10^{-5}$ T Å] [32]. This is an interesting feature because A^{3+}(VI)–O bonds are weaker than the M^{6+}(IV)–O ones and in a normal (positive) thermal expansion material these bonds generally possess a linear coefficient of thermal expansion (α) of around $6–8 \times 10^{-6}/^{\circ}C$ [33]. The absence of this expansion for A^{3+}(VI)–O in $Sc_2W_3O_{12}$, $Sc_2Mo_3O_{12}$ and $Y_2W_3O_{12}$ verified by Rietveld refinements is explained by transverse vibration mode of oxygen that compensates for the expected thermal expansion of A^{3+}(VI)–O bond lengths [16]. In $Cr_2Mo_3O_{12}$, however, the Cr–O bond length increases [d_{av}(Cr–O) = $1.9688 + 2.55 \times 10^{-5}$ T Å] as demonstrated in Fig. 6b. Nevertheless, it has to be considered that our study was carried out using an X-ray and not a neutron source, that would be preferable for the high accuracy of determination of oxygen positions and thus of metal–oxygen bond lengths. However, through smooth increase of isotropic temperature factors of Cr^{3+}, Mo^{6+} and O^{2-} as a function of temperature (see Supplementary information) it can be assessed [16,31] that the structural parameters of $Cr_2Mo_3O_{12}$ phase (for the temperature range 420–740 °C) refined through Rietveld method (see Supplementary information) formed a reliable structural model with no significant systematic flaws. Another indication of reliability of the structural model is based on good Rietveld reliability factors (Table 2) (mean standard uncertainties for Cr–O bond distances and Cr–Mo non-bond distances calculated by Rietveld refinements, Fig. 6, are at the same level as observed by Evans et al. [32] for $Sc_2Mo_3O_{12}$ from neutron diffraction data). Even if we take mean bond length of Cr–O at 740 °C (1.9903 Å) as a somewhat higher than expected and remove this point from the plot, it can be verified that the Cr–O mean bond length still increases with temperature [d_{av}(Cr–O) = $1.9775 + 7.79 \times 10^{-6}$ T Å] (Fig. 6b). Therefore, it can be rationalized that transverse vibrations of oxygen are not strong enough in orthorhombic $Cr_2Mo_3O_{12}$ phase (a near-zero thermal expansion material) to compensate for Cr–O bond length increase, as it is the case for $Sc_2W_3O_{12}$, $Sc_2Mo_3O_{12}$ and $Y_2W_3O_{12}$ phases (NTE materials). As a matter of fact, the mean non-bonding distance Cr–O–Mo is

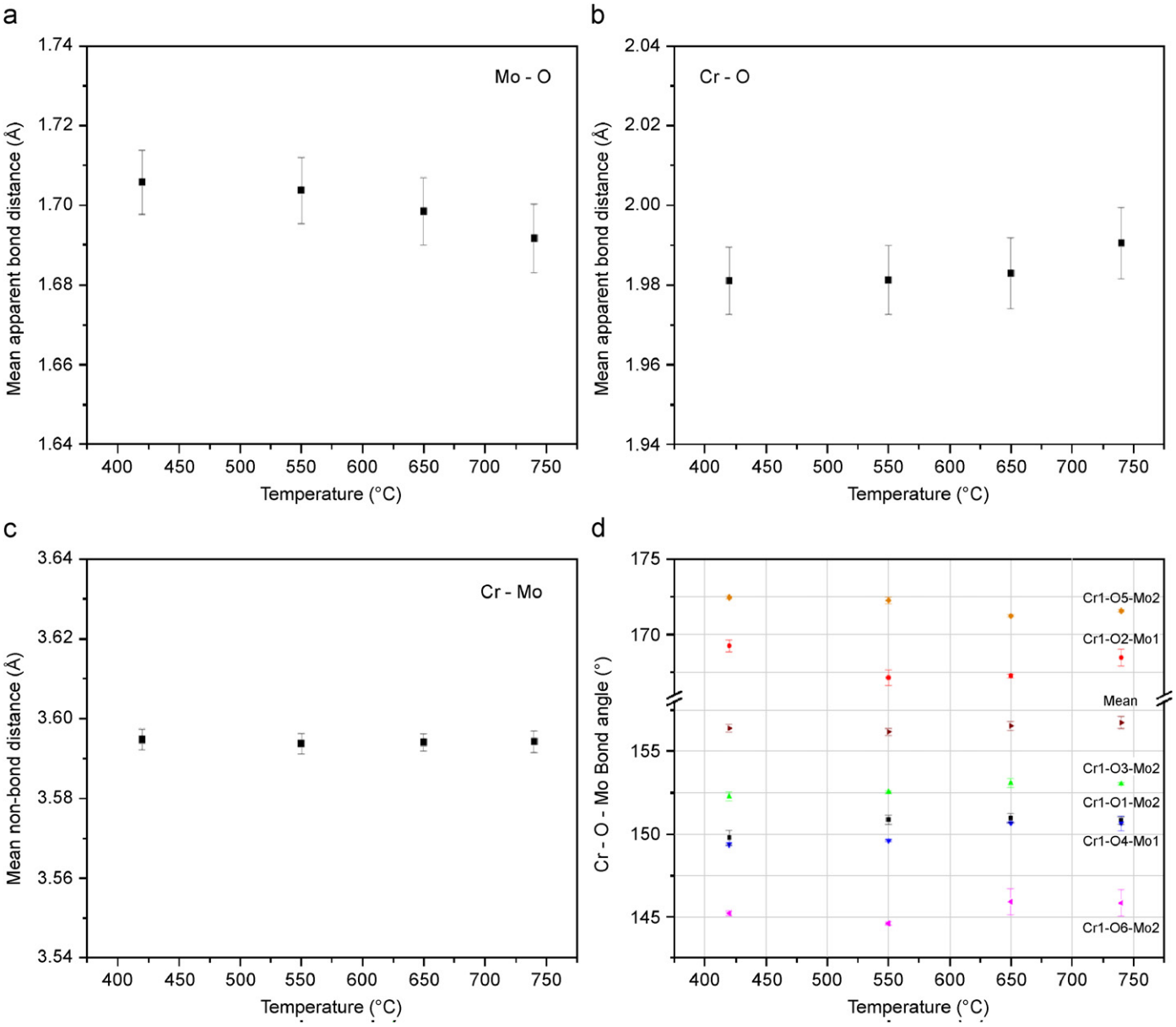

Fig. 6. Bond distances, non-bond distances and bond angles as a function of temperature for $Cr_2Mo_3O_{12}$ phase (a) mean apparent Mo–O bond distances, (b) mean apparent Cr–O bond distances, (c) Cr–Mo non-bond distances and (d) Cr–O–Mo bond angles.

maintained almost unchanged with increasing temperatures (Fig. 6c), which corroborates the conclusion that transverse vibrations of oxygen are not strong enough in orthorhombic $Cr_2Mo_3O_{12}$ phase to provoke a negative overall coefficient of thermal expansion. A lack of strong fluctuations in mean Cr–O–Mo bond angles can be confirmed as well, from Fig. 6d (standard uncertainties of the measured Cr–O–Mo angles are at the level of 0.25°, which is typical for Rietveld refinement results [31]). However, if one closely inspects each of the Cr–O–Mo angles it can be concluded that some of them increase and some others decrease with temperature. Since the crystal structure of $A_2M_3O_{12}$ family can be described as built from corner-shared polyhedra (AO_6 and MO_4) forming *bc* planes, being connected themselves along the ***a*** axis just through *A*–O3–*M*2 linkages, it can be assumed that the nature of *A*–O3–*M*2 angle variation with temperature influences thermal expansion along the crystallographic axis ***a***. It occurs that in $Cr_2Mo_3O_{12}$ this angle Cr1–O3–Mo2 increases with temperature (Fig. 6d). Therefore, it is reasonable that α_a is positive ($6.09\times10^{-6}/°C$). From five other angles, two of them, being Cr1–O2–Mo1 and Cr1–O5–Mo2, contract on heating. These are the very same angles that also contract in $Sc_2Mo_3O_{12}$ phase [32]. Actually, according to Evans and Mary [32] these two angles undergo abrupt increase on displacive phase transition from monoclinic to orthorhombic phase and therefore, these will be easily distort in orthorhombic phase, probably being responsible for NTE along the axes ***b*** ($-1.78\times10^{-6}/°C$) and ***c*** ($-2.47\times10^{-6}/°C$) in $Cr_2Mo_3O_{12}$.

4. Conclusions

Single-phased solid solutions were obtained for $Cr_{2x}Fe_{2-2x}Mo_3O_{12}$, $Al_{2x}Fe_{2-2x}Mo_3O_{12}$ and $Al_{2x}Cr_{2-2x}Mo_3O_{12}$ ($x=0$, 0.1, 0.3, 0.5, 0.7, 0.9 and 1). The relationship between cell parameters and the size of cation A^{3+} obeys Vegard's law for all solid solutions. The phase transition temperature increases with the A^{3+} cation electronegativity and there is a linear relationship between the transition temperature and the fraction of A^{3+} cations (x).

The thermal expansion coefficients for the orthorhombic phase and phase transition temperatures could be generally tailored by choosing larger or smaller A^{3+} cations. Nevertheless, our results showed that in some phases and solid solutions the A^{3+} cation size is not the only factor which influences the thermal expansion coefficient, as it is observed for $Cr_2Mo_3O_{12}$ and $Fe_2Mo_3O_{12}$.

Near-zero overall coefficient of thermal expansion of orthorhombic $Cr_2Mo_3O_{12}$ is tentatively explained in terms of temperature behavior of Mo–O and Cr–O bond lengths, Cr–O–Mo non-bond lengths and Cr–O–Mo angles.

Supplementary information

The atomic positions and isotropic thermal factors of orthorhombic $Cr_2Mo_3O_{12}$ at 420, 550, 650 and 740 °C have been deposited at the Fachinformationzentrum karlsruhe, Abt. PROKA, 76344 Eggenstein-Leopoldshafen, Germany, as supplementary material ICSD numbers 418845–418848 and can be obtained by contacting the FIZ quoting the article details or the corresponding ICSD number.

Acknowledgments

The authors are grateful to the Brazilian Synchrotron Light Laboratory (LNLS) for the beam time and financial support under the Projects D10B-XPD 5869/06 and D10B-XPD 5831/06.

M.S. Ari thanks CNPq and Capes for financial supports.

Appendix A. Supplementary information

Supplementary data associated with this article can be found in the online version at doi:10.1016/j.jssc.2008.03.015

References

[1] J.S.O. Evans, T.A. Mary, A.W. Sleight, Phys. B: Condens. Matter 241–243 (1998) 311–316.
[2] A.W. Sleight, Annu. Rev. Mater. Sci. 28 (1998) 29–43.
[3] A.W. Sleight, Inorg. Chem. 37 (1998) 2854–2860.
[4] J.S.O. Evans, J. Chem. Soc. Dalton Trans. (1999) 3317–3326.
[5] J.Z. Tao, A.W. Sleight, J. Solid State Chem. 173 (2003) 442–448.
[6] J.S.O. Evans, T.A. Mary, A.W. Sleight, J. Solid State Chem. 133 (1997) 580–583.
[7] J. Peng, M.M. Wu, H. Wang, Y.M. Hao, Z. Hu, Z.X. Yu, D.F. Chen, R. Kiyanagi, J.S. Fieramosca, S. Short, J. Jorgensen, J. Alloys Compd. 453 (2008) 49–54.
[8] M.M. Wu, J. Peng, Y.Z. Cheng, H. Wang, Z.X. Yu, D.F. Chen, Z.B. Hu, Solid State Sci. 8 (2006) 665–670.
[9] Y.Z. Cheng, M.M. Wu, J. Peng, X.L. Xiao, Z.X. Li, Z.B. Hu, R. Kiyanagi, J.S. Fieramosca, S. Short, J. Jorgensen, Solid State Sci. 9 (2007) 693–698.
[10] M.M. Wu, Y.Z. Cheng, J. Peng, X.L. Xiao, D.F. Chen, R. Kiyanagi, J.S. Fieramosca, S. Short, J. Jorgensen, Z.B. Hu, Mater. Res. Bull. 42 (2007) 2090–2098.
[11] M.M. Wu, J. Peng, Y.Z. Cheng, X.L. Xiao, Y.M. Hao, Z.B. Hu, Mater. Sci. Eng. B 137 (2007) 144–148.
[12] T.A. Mary, A.W. Sleight, J. Mater. Res. 14 (3) (1999) 912–915.
[13] V. Sivasubramanian, T.R. Ravindran, R. Nithya, A.K. Arora, J. Appl. Phys. 96 (1) (2004) 387.
[14] P.M. Forster, A. Yokochi, A.W. Sleight, J. Solid State Chem. 140 (1998) 157–158.
[15] D.A. Woodcock, P. Lightfoot, C. Ritter, J. Solid State Chem. 149 (2000) 92–98.
[16] P.M. Forster, A.W. Sleight, Int. J. Inorg. Mater. 1 (1999) 123–127.
[17] B.A. Marinkovic, P.M. Jardim, R.R. de Avillez, F. Rizzo, Solid State Sci. 7 (2005) 1377–1383.
[18] S. Sumithra, A.M. Umarji, Solid State Sci. 8 (2006) 1453–1458.
[19] A.K. Tyagi, S.N. Achary, M.D. Mathews, J. Alloys Compd. 339 (2002) 207–210.
[20] F.F. Ferreira, E. Granado, W. Carvalho Jr., S.W. Kycia, D. Bruno, R. Droppa Jr., J. Synchrotron Rad. 13 (2006) 46–53.
[21] W.M. Yim, R.J. Paff, J. Appl. Phys. 45 (1974) 1456–1457.
[22] R.D. Shannon, Acta Crystallogr. A 32 (1976) 751.
[23] V. Sivasubramanian, T.R. Ravindran, S. Kalavathi, A.K. Arora, J. Electroceram. 17 (2006) 57–60.
[24] A.L. Allred, J. Inorg. Nucl. Chem. 17 (1961) 2115–2221.
[25] K. Nassau, H.J. Levinstein, G.M. Loiacono, J. Phys. Chem. Solids 26 (1965) 1805–1816.
[26] Y.M. Yang, L.Ch. Li, M. Feng, Chin. J. Inorg. Chem. 23 (3) (2007) 382–386.
[27] J.S.O. Evans, T.A. Mary, T. Vogt, M.A. Subramanian, A.W. Sleight, Chem. Mater. 8 (12) (1996) 2809–2823.
[28] X.L. Xiao, Y.Z. Cheng, J. Peng, M.M. Wu, D.F. Chen, Z.B. Hu, R. Kiyanagi, J.S. Fieramosca, S. Short, J. Jorgensen, Solid State Sci. 10 (2008) 321–325.
[29] Z.X. Yu, J. Peng, H. Wang, M.M. Wu, Y.Z. Cheng, Z.B. Hu, D.F. Chen, Sci. China Ser. E—Tech. Sci. 51 (2008) 25–32.
[30] K.W. Chapman, P.J. Chupas, C.J. Kepert, J. Am. Chem. Soc. 128 (2006) 7009–7014.
[31] J.S.O. Evans, T.A. Mary, A.W. Sleight, J. Solid State Chem. 137 (1998) 148–160.
[32] J.S.O. Evans, T.A. Mary, Int. J. Inorg. Mater. 2 (2000) 143–151.
[33] R.M. Hazen, C.T. Prewitt, Am. Mineral. 62 (1977) 309–315.
[34] S. Sumithra, A.K. Tyagi, A.M. Umarji, Mater. Sci. Eng. B 116 (2005) 14–18.
[35] N. Imanaka, M. Hiraiwa, G. Adachi, H. Dabkowska, A. Dabkowski, J. Cryst. Growth 220 (2000) 176–179.
[36] S. Sumithra, A.M. Umarji, Mater. Res. Bull. 40 (2005) 167–176.